A combined theoretical and experimental study of the photophysics of asulam

Angelo Giussani,[†] Rosendo Pou-Amérigo,[†] Luis Serrano-Andrés,[†] Antonio Freire-Corbacho,[‡] Cristina Martínez-García,[‡] Mª Isabel Fernández P.,[‡] Moisés Canle L.,[‡] Mohamed Sarakha,[§] J. Arturo Santaballa,[‡]**

[†]Instituto de Ciencia Molecular, Universitat de Valencia, Ap. 22085 ES-46100, Valencia (Spain). [‡]Departamento de Química Física e Enxeñería Química I, Universidade da Coruña, Rúa da Fraga 10, ES-15008 A Coruña (Spain). [§]Laboratoire de Photochemie Moléculaire et Macromoléculaire, Université Blaise Pascal, UMR CNRS 6505, F-63177, Aubière Cedex (France).

Corresponding Authors

arturo.santaballa@udc.es & Angelo.Giussani@uv.es

Notes

Dr. Luís Serrano-Andrés deceased on September 2010.

A combined theoretical and experimental study of the photophysics of asulam

ABSTRACT

The photophysics of the neutral molecular form of the selective systemic herbicide asulam (methyl sulfanilylcarbamate) has been described in a joint experimental and theoretical, at the CASPT2 level, study. The unique absorption band (f c.a. 0.5), ascribed to a $\pi \rightarrow \pi^*$ aromatic electronic transition, shows a weak red-shift upon increasing the polarity of the solvent, but for water and ethanol, whereas the fluorescence band undergoes a larger red-shift as solvent polarity rises. Solvatochromic data have been analyzed in terms of models involving either bulk polarizability of the solvent or solute-solvent specific interactions (Kamlet-Abboud-Taft and Catalán et al.); results of the former point to higher dipole moment in the excited state than in the ground state ($\mu_g < \mu_e$), and the observed increase in pKa in the excited state (pKa* – pKa c.a. 3) is consistent with the results of the Kamlet-Abboud-Taft and Catalán et al.'s multiparametric approaches. Fluorescence quantum yield, at room temperature, varies with the solvent, being higher in water ($\phi_f = 0.16$) and lower in methanol and 1-propanol (aprox. 0.02). Fluorescence lifetime in aqueous solution at room temperature is (1.0 ± 0.2) ns ($k_f = 1.5 \cdot 10^{-8}$ s^{-1}), whereas the phosphorescence lifetime in glassy EtOH at 77 K and the corresponding quantum yield are (1.1 ± 0.1) s and 0.36 respectively, and, therefore, decay through non-radiative processes accounts for the remaining 48%. The lack of mirror image symmetry between modified absorption and

fluorescence spectra reflects different nuclear configurations in the absorbing and emitting states; the same conclusion is derived from both the experimental and theoretical dipole and transition dipole moments. The low value measured for the fluorescence quantum yield is justified by an efficient nonradiative decay channel, related with the presence of a conical intersection between the initially populated singlet bright $^1(L_a\ \pi\pi^*)$ state and the ground state, $(gs/\pi\pi^*)_{CI}$. Such conical intersection is easily accessible through a barrierless pathway from the initial state. Part of the population of the singlet state evolves along the main decay pathway and undergoes an internal conversion process that switches part of the population from the bright $^1(L_a\ \pi\pi^*)$ to the dark $1(L_b\ \pi\pi^*)$ state, which is responsible for the fluorescence of the system. Additionally, singlet-triplet crossing regions have been found along the minimum-energy decay path of the $^1(L_a\ \pi\pi^*)$ state, a fact which can explain the large triplet formation quantum yield determined in water ($\Phi_T = 0.84$), as well as the phosphorescent emission experimentally detected. An intersystem crossing region between the phosphorescence $^3(L_a\ \pi\pi^*)$ and the ground state has been characterised, which contributes to the nonradiative deactivation of the excitation energy.

KEYWORDS: photophysics, absorption, fluorescence, phosphorescence, laser flash photolysis, steady state irradiation, solvent effect, solvatochoromism, ab initio, computational chemistry, CASPT2//CASSCF, carbamate herbicide, excited state, linear solvation energy relationships, asulam.

Introduction

It is well known that used pesticides could either leach down to subsoil and contaminate the ground water, or persist on the top soil, thus becoming harmful to microorganisms, plants, and animals;[1]. Soil and groundwater pollution are the major environmental concern of pesticides application. The persistence in the environment of large quantities of pesticides, extensively used in agriculture, is known to have serious negative consequences for human health and for the equilibrium of ecosystems.[2]

Carbamates are large group of pesticides which have been extensively used for sixty years. More than 50 carbamates are known, which are effective as insecticides, herbicides, and fungicides, but they are most commonly used as insecticides. Herein we focus on the herbicide asulam, methyl((4-aminophenyl)sulfonyl)carbamate or N-(4-aminophenyl)sulfonylcarbamic acid methyl ester (see Figure 1).

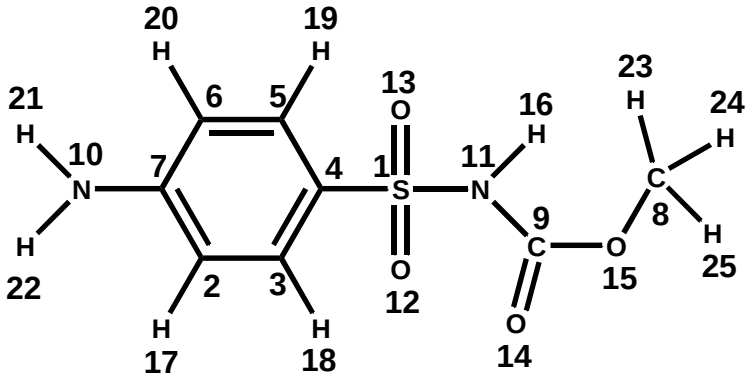

Figure 1. Structure, and atom numbering, of methyl [(4-aminophenyl) sulfonyl] carbamate (asulam)

Asulam, a selective systemic herbicide, is used for control of annual and perennial grasses and broad-leaved weeds in spinach, oilseed poppies, alfalfa, some ornamentals, sugar cane, bananas, coffee, tea, cocoa, coconuts, rubber, fruit trees and bushes, and forestry.[3,4]

This herbicide is highly mobile and has a strong potential to leach into ground water or move offsite into surface water. It is highly soluble in water, not volatile, stable in water without light, and unstable in water and on soil under light.[5] Technical asulam is practically nontoxic to freshwater fish, estuarine/marine species, honeybees, and small mammals, and poses minimal risk to freshwater invertebrates.[6]

There is an obvious need to develop new technologies able to remove pollutants in safer and cheaper ways. During the past decade water treatment technology moved towards advanced oxidation procedures, and, among the most successful procedures, the use of UV-light irradiation to trigger photodegradation of the toxic compounds has been found highly advantageous. Promoting the use of photodisposable chemicals can solve many of the already detected problems. Finding appropriate substances prompts for accurately establishing their photophysical and photochemical properties.

Solvent effects on UV–Vis absorption spectra can be used to determine the magnitude of the electric dipole moment of solute molecule in electronically excited state, provides information about the electronic and geometrical structure of the molecule in its short-lived excited state.

Contrary to the case of ground state, there are not many reliable techniques available for the estimation of the dipole moment of electronically excited states; among the existing methods, the most popular ones are based on a linear correlation between the wavenumbers of the absorption and fluorescence maxima ($\bar{\nu}_{a,max}$, $\bar{\nu}_{f,max}$) and solvent polarity functions, usually involving both the static dielectric constant (ε) and the refractive index (n) of the medium,[7] *i.e.* the solvatochromic method. UV-Vis absorption and emission spectra of a solute in different solvents can also be used to unravel solvation interactions at the molecular level in terms of multiparameter relationships like those due to Kamlet-Abboud-Taft [8-11] or to Catalán et al.[12]

Over the last decade the CASPT2//CASSCF methodology has been proven to be an efficient and reliable computational tool in order to study the photophysics and photochemistry of medium-size organic molecules. Such method is in fact able to provide a balanced description of the potential energy hypersurfaces of the excited states of a system along different nuclear conformations, and consequently allowed a coherent description of the deactivation processes that the molecule may undergo after UV absorption. The photoresponse of many basic chromophores have been in fact rationalised on the basis of quantum chemical CASPT2//CASSCF calculation, like for example the pyrimidines and purines nucleobases[13,14] as well as other relevant biological systems[15].

The purpose of the present research is to determine the photophysics of the systemic herbicide asulam by means of combined theoretical and experimental methodologies. Experimental measurements on the absorption and emission, both fluorescence and phosphorescence, spectra of asulam in different solvents and multiconfigurational quantum-chemical *ab initio* CASPT2 calculations on the low-lying singlet and triplet states will be employed to describe and rationalize the main population and decay pathways on the molecule upon UV irradiation.

Experimental and Computational Details

Experimental

Asulam -Methyl [(4-aminophenyl)sulfonyl] carbamate- (purity 96%), purchased from Riedel-de Häen, has been used as received; its purity was checked by HPLC and NMR. Aniline (Aldrich A.C.S reagent) has been further purified by microdistillation under nitrogen atmosphere.

Organic solvents, purchased from Sigma–Aldrich or Merck all of spectroscopic or HPLC quality, have been used as received, and did not show any traces of fluorescence. Water has been doubled distilled.

Steady-state UV−Vis absorption spectra have been recorded at room temperature on a Beckman DU-70 spectrophotometer with a wavelength accuracy of ± 0.1 nm. Fluorescence spectra have been recorded, also at room temperature, using a single beam spectrofluorimeter (Aminco-Bowman Series 2) equipped with a 150 W continuous Xenon lamp. For all spectral measurements the solutions have been kept in Suprasil quartz cells of 1 cm light path.

Fluorescence quantum yields (ϕ_f) have been calculated using the comparative method,[16] with aniline as standard,[17] according to the following equation:

$$\phi_f^i = \phi_f^s \frac{A_s}{A_i} \frac{I_f^i(\lambda)}{I_f^s(\lambda)} \frac{n_i^2}{n_s^2}$$

where i and s refer to asulam and standard, respectively; A is the absorption at the excitation wavelength (282 nm); I_f stands for the fluorescence intensity, and n represents the refractive index of the solvent. Low concentration has been used (ca. $8.0 \cdot 10^{-6}$ mol·dm^{-3}) ensuring that the approximations involved in the above equation are met.

The demodulation and phase shift measurements of fluorescence lifetimes have been done using a Single Photon Counting SLM 48000™S Multiple Frecuency Lifetime Spectrofluoremeter SIM AMINCO® equipped with a 450 W Xenon lamp as light source. Lifetime measurements, in the range 20 ps to 1.58 ms, have been done at different modulation frequencies between 10 kHz to 2 GHz.

The low-temperature phosphorescence spectra of asulam as well as of benzophenone have been recorded at 77 K in glassy EtOH using a single beam spectrofluorimeter (Aminco-Bowman

Series 2) equipped with a 7 W pulsed Xenon lamp, with exciting irradiation at 282 nm and the emission collected at 404 nm. The phosphorescence decay curves were analyzed as mono exponentials, and the phosphorescence decay time (τ_P) has been obtained from the slope of the linearlized first order plot.

Computational

The present calculations include CASSCF geometry optimizations, minimum energy paths (MEP), and conical intersection and singlet-triplet crossing searches, followed by multiconfigurational perturbation theory (CASPT2) calculations at the optimized geometries, using a standard zeroth-order Hamiltonian.[18,19] An imaginary level shift of 0.1 au has been employed to prevent the presence of intruder states. Spin-orbit coupling terms and transition dipole moments have been also computed. The final results involve an active space of 6 electrons distributed in 6 orbitals, CASPT2(6,6)//CASSCF. A one-electron basis set of the ANO-S type contracted to S[4s3p1d]/C,N,O[3s2p1d]/H[2s] has been used throughout. The ground state and the Onsager cavity radius, however, used a geometry optimized at the DFT/B3LYP/6-31G(d) level of calculation. MEPs have been built as steepest-descendent paths in which each step required the minimization of the energy on a hyperspherical cross section of the PEH centered on the initial geometry and characterized by a predefined radius. Conical intersections and singlet-triplet crossings have been computed as minimum energy crossing points (MECP) on the PEH.[20,21] No spatial symmetry restrictions were imposed. More detailed technical aspects of the calculations can be found in the Supporting Information (SI). The calculations reported used the quantum chemical methods implemented in the MOLCAS 6.4 package,[22] and in Gaussian 09 suite.[23]

Results and discussion

A. Steady-state absorption and fluorescence spectra

Asulam could exist in three forms in aqueous solution (Figure 2), their relative concentration depending on the acidity of the medium.[24]

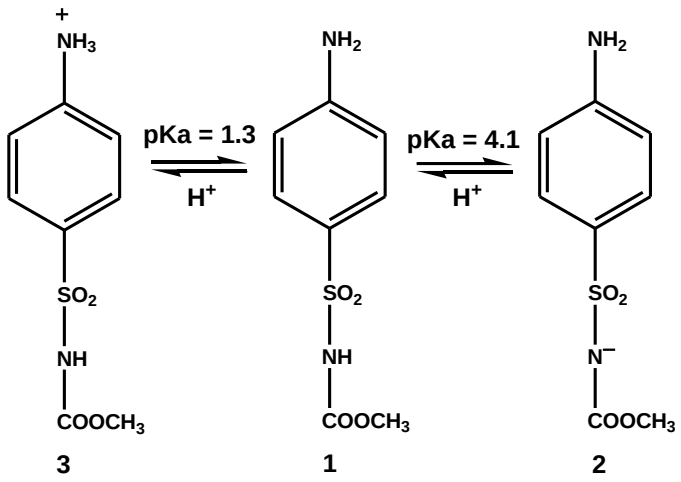

Figure 2. Acid-base equilibria of asulam in aqueous solution

Room temperature UV–Vis absorption and fluorescence spectra of asulam have been measured in different solvents. The electronic (UV–Vis) absorption spectra of the molecular form of asulam (1) in water, ethanol (Fig. 3) and other organic solvents show one intense structureless band with a well defined peak, which highlights a $\pi \rightarrow \pi^*$ electronic transition.

The steady-state absorption spectra of **1** show a relatively small solvent effect on the position and shape of the absorption band (Table 1). Bathochromic shifts are observed as solvent polarity increases, but for ethanol and water. Because of its large molar absorption coefficient (ε_{max}), e.g. in water 16836 $mol^{-1} \cdot dm^3 \cdot cm^{-1}$ at λ_{max} = 256 nm, that absorption band, located in the 255–270 nm region, was attributed to $\pi \rightarrow \pi^*$ aromatic electronic transitions, similar to that of aniline.[25]

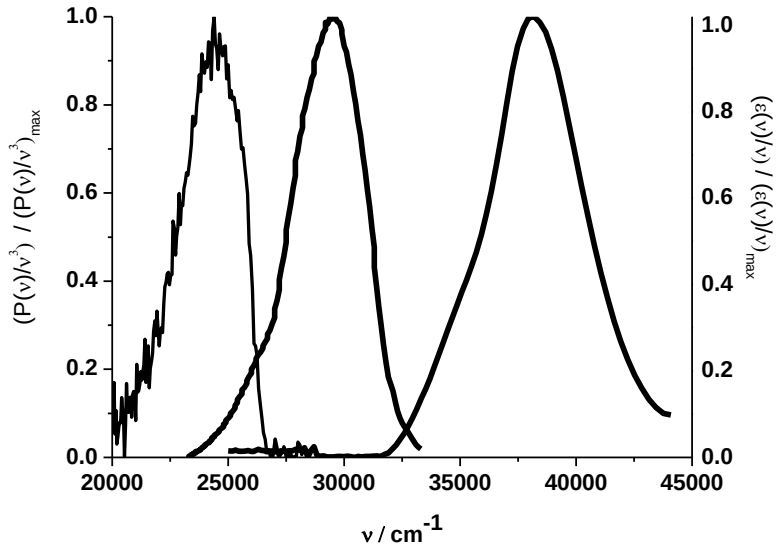

Figure 3. Steady-state spectra of the molecular form of asulam (**1**) in ethanol. From the left to the right: phosphorescence (low temperature -77 K-), fluorescence and UV-Vis absorption (T ca 293K). ([asulam]= 16 μM).

The intrinsic ability of a molecule to absorb light is often expressed in terms of the oscillator strength for the electronic transition (*f*), which can be determined experimentally by integrating the molar absorptivity over the frequency ν (in cm^{-1}) according to the following equation:[26]

$$f = \frac{4.39 \cdot 10^{-9}}{n} \cdot \int_{\bar{\nu}_1}^{\bar{\nu}_2} \varepsilon(\bar{\nu}) d\bar{\nu}$$

where the molar absorptivity, $\varepsilon(\bar{\nu})$, has units of $dm^3 \cdot mol^{-1} \cdot cm^{-1}$ and the frequency, ν, is in wave number (cm^{-1}). This integration extends from $\bar{\nu}_1$ to $\bar{\nu}_2$, which are the limits of the band associated with the electronic transition from lower to upper state, and n stands for the refractive

index of the solvent. Values of *f* in water, neutral and acid conditions, and in ethanol were 0.48 and 0.50 respectively, implying a strong transition.

The best quantitative measure of the transition probability, the transition dipole moment ($\mu_{g\to e}$), has been obtained in terms of the oscillator strength by using the expression:[27]

$$\mu_{g\to e} = \sqrt{\frac{3 \cdot h \cdot e^2 \cdot f}{8 \cdot \pi^2 \cdot m_e \cdot c \cdot \bar{\nu}_{a,max}}}$$

where e is the elementary charge, m_e the electron mass, c the light speed in vacuum, and h the Planck's constant. Assuming the electronic degeneracies of the lower and upper state are the same, 5.3 D (ethanol) and 5.2 D (water) have been estimated for the transition dipole moment $\mu_{g\to e}$.

Room temperature UV–Vis fluorescence spectra of the molecular form of asulam (**1**) in some organic solvents is shown in Fig. SI1 of SI, and the corresponding maxima ($\bar{\nu}_{f,max}$) and Stokes' shifts ($\bar{\nu}_{a,max} - \bar{\nu}_{f,max}$) collected in Table 1. The presence of the amino group is responsible of fluorescence as benzenesulphonamide does not show it, but it is present in the closely related sulphanilamide.[28] As for the absorption spectra, small solvent effects on the position and shape of the structureless band are observed; this time, red shifts take place when the polarity of the solvent is increased.

Room temperature UV–Vis fluorescence spectra of the molecular form of asulam (**1**) in some organic solvents is shown in Fig. SI1 of SI, and the corresponding maxima ($\bar{\nu}_{f,max}$) and Stokes' shifts ($\bar{\nu}_{a,max} - \bar{\nu}_{f,max}$) collected in Table 1. The presence of the amino group is responsible of fluorescence as benzenesulphonamide does not show it, but it is present in the closely related sulphanilamide.[28] As for the absorption spectra, small solvent effects on the position and shape

of the structureless band are observed; this time, red shifts take place when the polarity of the solvent is increased.

Table 1. Solvent effects on the electronic absorption and fluorescence spectral data of the molecular form of asulam (**1**)[a]

Solvent	$\bar{\nu}_{a,max}$ cm^{-1}(nm)	$\bar{\nu}_{f,max}$ cm^{-1}(nm)	($\bar{\nu}_{a,max}$ -$\bar{\nu}_{f,max}$)/cm^{-1}
Dichloromethane	37594 (266)	30864 (324)	6730
Trichloromethane	37736 (265)	30864 (324)	6872
Propan-1-ol	37313 (268)	29761 (336)	7552
Acetonitrile	37313 (268)	30030 (333)	7283
Methanol	37453 (267)	29673 (337)	7780
Ethanol	38197 (262)	29762 (336)	8435
Ethylene glycol	36900 (271)	29761 (336)	7139
1,4-Dioxane	37594 (266)	30211 (331)	7383
Diethyl ether	37453 (267)	30487 (328)	6966
Water	39216 (255)	29412 (340)	9804

[a] T ca 293 K

Frequency of electronic 0–0 transition between the ground state and the excited singlet state of molecules has been determined from abscissa corresponding to intersection point of modified absorption spectrum, $\varepsilon(\bar{\nu})/\bar{\nu}$ versus $\bar{\nu}$, and normalized modified fluorescence spectrum, $I_F(\bar{\nu})/\bar{\nu}^3$ versus $\bar{\nu}$,[29] where $\bar{\nu}$ is the wavenumber (in cm^{-1}). Similar values have been found for such 0–0 transition in water and in ethanol, 307 and 306 nm respectively; on the other hand, crossing between fluorescence and phosphorescence bands takes place at 380 nm (Fig. 3). No mirror

image symmetry exists between the absorption and fluorescence spectra (Fig. 3), indicating that the geometry of the molecular form of asulam (**1**) in the emitting and absorbing states is not the same.[30,31]

Fluorescence spectra is more sensitive to the nature of the solvents, which points to greater charge transfer taking place from amino group to the aromatic ring in the excited state in comparison to the ground state, and also to a dipole moment larger in the excited state than S_0. For aniline noticeable solvent-induced shifts in the maximum of fluorescence have been observed;[32] and the Stokes shift between absorption and fluorescence maxima varies with the polarity of the solvent.

The anionic form of asulam (**2**) also shows fluorescence, the corresponding room temperature steady–state spectrum as well as that of absorption are depicted in Fig. SI2 of SI. The absorbance maximum of **2** moves to higher wavelength (λ_{max} = 268 nm) relative to the neutral form (**1**), its shape and intensity remaining nearly unchanged. On the other hand, the emission spectra of **1** & **2** show an almost coinciding broad band, that of **2** three-fold less intense than that of **1**. The coincidence of the fluorescence peaks of the anionic and molecular forms is usually observed in sulfonamides.[33] The pK_a of the excited state could be estimated by using the absorption data of the molecular and the anionic forms in the Förster's cycle.[34] The pK_a in the excited state (pK_a*) increases 3.1 units, *i.e.* excited asulam becomes more basic; the same behavior has been reported for sulfonylureas, which show similar acid-base chemistry.[24]

This behavior is opposite to that of aniline, where a decrease of c.a. 8 units is observed;[35] notice the deprotonation leads to a negatively charged species (**2**) for asulam, whereas aniline becomes neutral.

The phosphorescence spectrum of the molecular form of asulam (**1**) shows a blurred and unsymmetrical band with its maximum located at 405 nm (Fig. 3). Phosphorescence of sulfanilamide and some derivatives in the same matrix, and temperature, occurs in the same region (405 – 420 nm),[33,36] and it could be assigned as a $\pi^* \rightarrow \pi$ transition from the lowest triplet state.[33]

Photophysics

The measured fluorescence quantum yields, in some organic solvents and under different acidity conditions in water, the molecular form of asulam (**1**) are collected in Table 2. No clear trend is observed with either the polarity of the solvent or the acidity. Aqueous solutions show the highest fluorescence quantum yield, which implies that the presence of water provokes a decrease in the rate of the non-radiative channels.

Apart from water, the higher quantum yields of **1** are observed in diethyl ether and dioxan. The reason for the value observed in dioxane was justified by Forbes for aniline, which shows similar results.[39] They suggested the formation of an aniline-dioxan interaction that enhances ϕ_f (a higher degree of e^--transfer from the N to the ring, that allows a higher population on the excited state). A similar explanation should be feasible for ethyl ether.

In the case of water, Kochemirovskii,[40] Blais and Gauthier[41] obtained for aniline a decrease of quantum yield with respect to organic solvents not containing hydroxyl groups; the interaction between water and the non-bonding electrons of the amino nitrogen, forming a 1:1 complex, leading to such decrease. However, in case of asulam, the quantum yield in water is the largest (Table 2), a possible explanation being the presence of the electron-withdrawing sufonyl group, implying a weaker interaction with the non-bonding electrons of the amino nitrogen (Figure 4).

Table 2. Fluorescence quantum yield of asulam, ϕ_f, using the comparative method with aniline as reference (λ_{exc} = 282 nm, T = 293K).

			pH					
Solvent			3.21	6.52	7.80	9.09	10.2	10.9
1,4-Dioxane	0.057							
Diethyl ether	0.099							
Methanol	0.023							
Water	0.155	0.032**	0.186	0.201	0.189	0.171	0.190	0.165
Acetonitrile	0.032	0.15*						
Propan-1-ol	0.025							

* Ref. 37

** Ref. 38

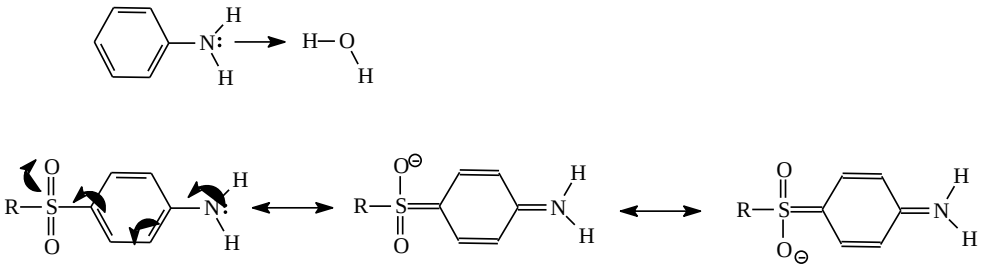

Figure 4. Resonant structures non present in aniline

The non-bonding electrons of the nitrogen atom in aniline are more readily available than in the case of asulam, in which the interaction with water is more difficult, the net effect being a larger value of the quantum yield.

Single photon counting measurements allowed the estimation of the fluorescence lifetime, τ_f = (1.0 ± 0.2) ns, of the molecular form of asulam (**1**) in aqueous solution (see Table SI1 of SI).

Taking into account the fluorescence quantum yield and the fluorescence lifetime, the natural fluorescence lifetime (τ_f^0) could be obtained as:

$$\tau_F^0 = \frac{\tau_f}{\Phi_f} = \frac{1}{k_f}$$

In aqueous solution τ_f^0 is 6.5 ns, thus a monoexponential fluorescence decay rate constant (k_f) of $1.5 \cdot 10^8$ s^{-1} is obtained; this value compares not too bad with $6 \cdot 10^8$ s^{-1}, calculated from the observed absorption and fluorescence bands using the Stricler-Berg approximation:[42]

$$k_f = \frac{1}{\tau_F^0} = 2.88 \cdot 10^{-9} \cdot n^2 \cdot \frac{\int F(\bar{\nu}) d\bar{\nu}}{\int \frac{F(\bar{\nu})}{\bar{\nu}^3} d\bar{\nu}} \cdot \int \frac{\varepsilon(\bar{\nu})}{\bar{\nu}} d\bar{\nu}$$

where n is the refractive index, $\bar{\nu}$ wave number (cm^{-1}), $\varepsilon(\bar{\nu})$ the molar absorptivity, and $F(\bar{\nu})$ the fluorescence intensity. Stricler-Berg's approximation is strictly valid when the ground and excited electronic states possess the same geometry; furthermore, it is well known that the Strickler-Berg approximation is not applicable to systems with predominant non-radiative pathways.[26,42,43]

The intrinsic radiative decay rate constant of fluorescence is also related to the fluorescence dipole transition moment:[29]

$$\mu_{e \to g} = \sqrt{\frac{3 \cdot h \cdot \Phi_f}{64 \cdot \pi^4 \cdot n^3 \cdot \tau_f \cdot \nu_{f,max}^3}}$$

a value of 2.1 D is found in aqueous solution, far from 5.2 D obtained for the ground to excited state transition dipole moment (*vide supra*), suggesting electronic and geometrical relaxation in the excited state.

Although there is no phosphorescence (P) at room temperature, it is observed in EtOH at 77K (see Fig. 3). The normal phosphorescence quantum yield (ϕ_P), i.e. the singlet photon absorption induced phosphorescence quantum yield, is given by:

$$\Phi_P = \frac{n_{ph,P}}{n_{ph,abs}} = \Phi_{ISC} \cdot \Phi'_P = \Phi_{ISC} \frac{\tau_P}{\tau_P^0}$$

where $n_{ph,P}$ is the total number of emitted phosphorescence photons, and $n_{ph,abs}$ is the total number of absorbed excitation light photons, Φ_{ISC} stands for is the quantum yield of singlet-triplet intersystem-crossing, Φ'_P is the intrinsic, triplet based, phosphorescence quantum yield, τ_P and τ_P^0 are the phosphorescence and intrinsic phosphorescence lifetimes respectively.

The obtained values for the phosphorescence lifetime and quantum yield of the molecular form of asulam (**1**) are (1.1 ± 0.1) s and 0.36 (using benzophenone as reference with ϕ_P = 0.84[17]) respectively. Assuming intersystem crossing (ISC) prevails over internal conversion (IC),[44] the excited states coming to the triplet state are equal to (1 - Φ_f), therefore the intrinsic phosphorescence lifetime (τ_P^0) is estimated from:

$$\tau_P^0 = \tau_P \left(\frac{1 - \Phi_f}{\Phi_P} \right) = \frac{1}{k_P}$$

the calculated τ_P^0 is 2.6 s, and therefore 0.4 s^{-1} is obtained for the intrinsic monoexponential phosphorescence decay rate constant (k_P) of the molecular form of asulam (**1**) in ethanol at 77 K. Similar phosphorescence lifetimes have been obtained for sulfanilamide and derivatives.[36]

Taking into account those results, the value for Φ_{ISC} is 0.84, and the corresponding monoexponential intersystem crossing rate constant being $8.7 \cdot 10^9$ s^{-1}.

Photophysics results imply that 16% of asulam molecules (**1**) deactivate by fluorescence, 36% through phosphorescence, and the remaining 48% uses non-radiative decay pathways, mainly from the triplet state.

The quenching effect of molecular oxygen ($^3O_2$) is variable, noticeable in 1-propanol and small in water (Table SI2 of SI). From the slope of the corresponding Stern-Volmer plot (Fig. SI3 of SI), the bimolecular quenching rate constant, for molecular oxygen in aqueous solution, is $1.4 \cdot 10^{10}$ $mol^{-1} \cdot dm^3 \cdot s^{-1}$.

Solvent effects

Solvatochromic Measurements and Dipole Moments.

The purpose of the study of steady-state Stokes shifts is to distinguish between solvent-induced shifts and spectral shifts due to intramolecular relaxation. Interactions between solute and solvent are responsible for the Stokes shifts, i.e. the observed solvatochromism. This approach relies on the possibility to describe each solvent by one or several parameters reflecting the solvent effect on the spectra.

The excited state dipole moment can be calculated from the solvatochromic shifts of the absorption and fluorescence spectra by the solvatochromic method,[12,46-49] which involves inexpensive equipment, and reflects the effect of electric field on the position change of the absorption and emission bands. Solvatochromic shifts in absorption give information only on the variation of solvation energy occurring immediately after the molecular excitation, thus not reflecting time averaged effects that would eventually result from subsequent events. The red

shift of the absorbing and emitting bands with increasing solvent polarity indicates that the excited state dipole moment (μ_e) is higher than that of the ground state (μ_g).

Solvatochromic data are usually analyzed by variants of the method first proposed by Lippert and Mataga,[50-53] who evaluated the change in dipole moment ($\Delta\mu = \mu_e - \mu_g$) in going from the ground state (g) to the excited state (e) through a plot of the Stokes shift as a function of a macroscopic solvent polarity parameter, and obtaining μ_g from another source, either theoretical or experimental. Here the following equations have been used:

Ooshika-Lippert-Mataga: $\bar{\nu}_{a,max} - \bar{\nu}_{f,max} = m_1 \cdot f_0(\varepsilon, n) + (\bar{\nu}_{a,0} - \bar{\nu}_{f,0})$

Bakshiev: $\bar{\nu}_{a,max} - \bar{\nu}_{f,max} = m_2 \cdot f(\varepsilon, n) + (\bar{\nu}_{a,0} - \bar{\nu}_{f,0})$

Kawski-Chama-Viallet: $\bar{\nu}_{a,max} + \bar{\nu}_{f,max} = -m_3 \cdot \Phi(\varepsilon, n) + (\bar{\nu}_{a,0} + \bar{\nu}_{f,0})$

with $\Phi(\varepsilon, n) = f(\varepsilon, n) + 2 \cdot g(n)$, and

$$m_1 = \frac{2 \cdot (\mu_e - \mu_g)^2}{4 \cdot \pi \cdot \varepsilon_0 \cdot h \cdot c \cdot a^3} \qquad m_2 = \frac{2 \cdot (\mu_e - \mu_g)^2}{4 \cdot \pi \cdot \varepsilon_0 \cdot h \cdot c \cdot a^3} \qquad m_3 = \frac{2 \cdot (\mu_e^2 - \mu_g^2)}{4 \cdot \pi \cdot \varepsilon_0 \cdot h \cdot c \cdot a^3}$$

where $\bar{\nu}_{a,max}$ and $\bar{\nu}_{f,max}$ designate the wave numbers of the peak absorbance and fluorescence, respectively; ε and n are the static electric relative permittivity and the refractive index of the solvent, correspondingly; c denotes the light speed in vacuum, ε_0 is vacuum permittivity; h is the Planck constant, a refers to the effective radius of the Onsager spherical cavity for the solute, and $(\bar{\nu}_{a,0} - \bar{\nu}_{f,0})$ is the difference of the frequencies of the peaks of the absorption and emission spectra in the case of zero solute-solvent interaction, i.e., the purely intramolecular contribution.

Taking into account Onsager's model, the simplest quantum-mechanical second order perturbation theory, assuming the condition $\alpha/a^3 = 0.5$ is fulfilled, being α the isotropic

polarizability of the solute, and that the symmetry of the solute remains unchanged upon electronic transition, the solvent functions of bulk solvent properties $f_0(\varepsilon, n)$, $f(\varepsilon, n)$, and $g(n)$ are:

$$f_0(\varepsilon, n) = \left(\frac{\epsilon - 1}{2\epsilon + 1} - \frac{n^2 - 1}{2n^2 + 1}\right)$$

$$f(\varepsilon, n) = \frac{2n^2+1}{n^2+2}\left(\frac{\epsilon-1}{\epsilon+2} - \frac{n^2-1}{n^2+2}\right) \text{ and } g(n) = \frac{3}{2}\frac{n^4-1}{(n^2+2)^2}$$

When the dipole moments of the ground and excited states are not parallel, the following equations relate them:

$$\mu_e = \left(\mu_g^2 + \frac{1}{2} m_2 4\pi\epsilon_0 hca^3\right)^{\frac{1}{2}}$$

$$cos\beta = \frac{1}{2\mu_e\mu_g}\left[\left(\mu_e^2 + \mu_g^2\right) - \frac{m_1}{m_2}\left(\mu_e^2 - \mu_g^2\right)\right]$$

Static electric relative permittivity and the refractive index of the solvents used in this study are collected in Table SI3 of SI. Figs. SI4 – SI6 of SI show the graphs of Stokes shift versus bulk solvent polarity function according to Ooshika-Lippert-Mataga, Bakhshiev and Kawski-Chama-Viallet equations, respectively; from those graphs m_1, m_2 and m_3 are obtained (Table 3). Linear fits were not good, even excluding data from water, 1,4-dioxane and ethanol. Poor fit has been also described for aniline, 1,4-dioxane behaving as outlier.[54]

Table 3. Parameters of the least squares fittings of solvatochromic data to mono and multiparameter linear solvation energy relationships

Ooshika-Lippert-Mataga	$\bar{\nu}_{a,max} - \bar{\nu}_{f,max} = (\bar{\nu}_{a,0} - \bar{\nu}_{f,0}) + m_1 \cdot f_0(\varepsilon, n)$					r	F
	$(\nu_{0,A} - \nu_{0,F})$ / cm^{-1}		m_1 / cm^{-1}			0.76	
	6126	± 413	4390	± 1657		(n = 7)	
Bakhshiev	$\bar{\nu}_{a,max} - \bar{\nu}_{f,max} = (\bar{\nu}_{a,0} - \bar{\nu}_{f,0}) + m_2 \cdot f(\varepsilon, n)$						
	$(\nu_{0,A} - \nu_{0,F})$ / cm^{-1}		m_2 / cm^{-1}			0.71	
	6385	± 374	1206	± 535		(n = 7)	
Kawski-Chama-Viallet	$\bar{\nu}_{a,max} + \bar{\nu}_{f,max} = (\bar{\nu}_{a,0} + \bar{\nu}_{f,0}) - m_3 \cdot \Phi(\varepsilon, n)$						
	$(\nu_{0,A} + \nu_{0,F})$ / cm^{-1}		m_3 / cm^{-1}			- 0.78	
	70904	± 1218	2770	± 1008		(n = 7)	
Reichardt	$\bar{\nu}_{a,max} - \bar{\nu}_{f,max} = (\bar{\nu}_{a,0} - \bar{\nu}_{f,0}) + m_4 \cdot E_T^N$						
	$(\nu_{0,A} - \nu_{0,F})$ / cm^{-1}		m_4 / cm^{-1}			0.73	
	6427	± 437	2276	± 747		(n = 10)	
Kamlet-Taft	$\bar{\nu}_{max} = \bar{\nu}_0 + a \cdot \alpha + b \cdot \beta + p \cdot \pi^*$						
Absorption	$\nu_{0,A}$ / cm^{-1}	a_A	b_A	p_A		0.25*	0.594
	37910	1020	-1299	- 227		(n = 10)	
	± 1373	± 1090	± 1766	± 1685			
Emission	$\nu_{0,F}$ / cm^{-1}	a_E	b_E	p_E		0.886*	0.003
	31641	-73	-1673	554		(n = 10)	
	± 431	± 342	± 1094	± 529			
Catalan et al.	$\bar{\nu}_{max} = \bar{\nu}_0 + csa \cdot SA + csb \cdot SB + csp \cdot SP + cdsp \cdot SdP$						
Absorption	$\nu_{0,A}$ / cm^{-1}	csa_A	csb_A	csp_A	$csdp_A$	0.697*	0.139
	42189	1220	-1964	- 4563	-1300	(n = 10)	
	± 2248	± 568	± 729	± 2690	± 922		

Emission	$\nu_{0,F}$ / cm^{-1}	csa_E	csb_E	csp_E	$csdp_E$	0.852*	0.026
	29510	-1006	- 544	1834	-190	(n = 10)	
	± 1259	± 318	± 408	± 1506	± 516		

* R-squared (coefficient of determination)

The deviation in dioxane is consistent with the fact that dioxane acts as a pseudopolar solvent of variable polarity function, which depends upon the solute's electric field, as a result of conformation polarizability.[55] The peculiar behavior in dioxane has been already described in the literature, e.g. aniline and derivatives,[32] and coumarins.[56]

Likewise aniline, solvent effects on the spectra enables us to consider specific solvent effects of water on asulam; the observed red-shift in its absorption band in polar solvents is ascribable to an increase in dipole moment upon excitation. Blue shift is observed in aqueous solutions in spite of its highly polar nature, which could be due to a lowering of hydrogen bond stabilization of the excited state relative to the ground state.

The angle between the dipole moment of the emitting state and of the ground state is 25º, the former being higher than the latter by 2.3 D, *i.e.* μ_e = 7.8 D, which is consistent with the observed red shift of the absorption and emitting bands with the polarity of the solvent. The dipole moment of the ground state was calculated theoretically, 5.51 D, using the CASPT2(6,6)//CASSCF method and a one-electron basis set of the ANO-S type contracted to S[4s3p1d]/C,N,O[3s2p1d]/H[2s]. Table 4 shows the obtained values of μ_e and μ_g assuming collinearity, and $\Delta\mu$ using Ooshika-Lippert-Mataga equation, again $\mu_e > \mu_g$.

Solvent effects on the absorption and emitting bands of the molecular form of asulam (**1**) do not follow the classical behavior with bulk polarity functions, which suggests that specific solute-solvent interactions are not negligible. Intuitively, from the molecular structure of asulam,

the oxygen atoms in sulfonyl and carbonyl groups, and the lone pair electron on the nitrogens can act as hydrogen bond acceptors, moreover, the hydrogen atoms in the nitrogens can act as hydrogen bond donors; thus, water and alcohols shows amphipathy in the hydrogen-bonding system (Fig. 5), whereas aprotic solvents can form hydrogen bonds with hydrogen bond donor sites in asulam, but cannot interact with hydrogen bond acceptor sites.

Table 4. Dipole moments of the ground (μ_g) and excited state (μ_e) calculated theoretically and with the solvatochromic method (assuming they are collinear)

	a[a] / Å	μ_g[b] / D	μ_e[b,c] / D	μ_g[d] / D	μ_e[d] / D	μ_e/μ_g[d]	$\Delta\mu$[d] / D	$\Delta\mu$[e] / D	$\Delta\mu$[f] / D
Value	4.83	5.51	8.70	2.4	6.1	2.5	3.7	7.0	2.8

[a] Theoretical calculation -B3LYP/6-31G(+)-; [b] Theoretical calculation -CASPT2-; [c] S_2 level, Theoretical calculation -CASPT2-; [d] Using Bakhshiev & Kawski-Chama-Viallet eqs.; [e] From Lippert-Mataga eq.; [f] Using Reichardt eq.

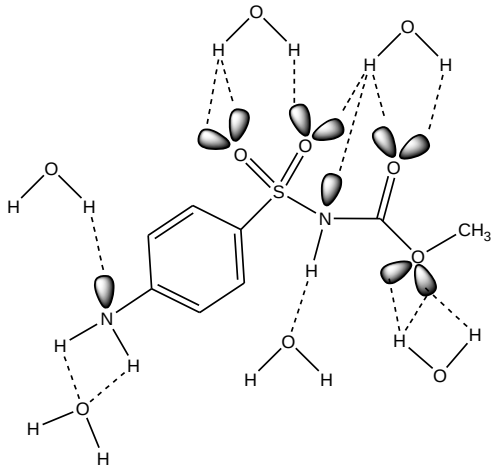

Figure 5. Simplified view of the possible hydrogen bonds involved in the ground and excited states of asulam (**1**) in aqueous solution

A multitude of empirical single- and multi-parameter solvent scales designed on the basis of solvent-dependent phenomena (spectroscopic, kinetic, equilibrium) have been proposed to quantify solvation interactions at molecular level.[48]

These scales could be based on one single parameter, like the so-called Dimroth-Reichardt;[48] or involving multiparametric correlation equations, either by the combination of two or more existing scales or by postulating specific parameters, to unravel the effect of the medium, e.g. Kamlet *et al.* (α, β and π* parameters) [8-11] or Catalán *et al.* (SP, SdP, SB and SA).[12]

Sometimes solvatochromic shifts of dipolar molecules correlate better with microscopic solvent polarity parameters, such as the dimensionless microscopic solvent polarity parameter E_T^N proposed by Reichardt,[48] rather than traditionally used bulk solvent polarity functions involving relative permittivities and refractive indices (*vide supra*); this parameter also considers interactions of specific

character in addition to the non-specific solvent effects. In this method the change in dipole moment ($\Delta\mu = \mu_e - \mu_g$) is calculated from the plot of Stokes shifts ($\bar{\nu}_{a,max} - \bar{\nu}_{f,max}$) versus E_T^N of the solvents according to the following equation:

$$\bar{\nu}_{a,max} - \bar{\nu}_{f,max} = m_4 \cdot E_T^N + (\bar{\nu}_{a,0} - \bar{\nu}_{f,0})$$

where E_T^N is a solvatochromic parameter based on the absorption wavenumber of a standard betaine dye in the corresponding solvent. Values of E_T^N for the solvents used here are collected in Table SI3 of SI.

The change in dipole moment relates to the slope m_4 as:

$$\Delta\mu = \mu_e - \mu_g = \sqrt{\frac{m_4 \cdot 81}{\left(\frac{6.2}{a}\right)^3 \cdot 11307.6}}$$

the meaning of $\bar{\nu}_{a,max}$, $\bar{\nu}_{f,max}$ and a is the same as previous equations.

A linear dependence of Stokes shifts versus E_T^N was obtained for the ten solvents used in this study (Fig. SI6 of SI), which is a clear evidence of the existence of specific solute–solvent interactions. From the slope m_4 (Table 3), the difference between dipole moments ($\mu_e - \mu_g$) is 2.8 D, which is consistent with that obtained using bulk solvent polarity functions.

The empirical Kamlet-Abboud-Taft (α, β and π*),[8-11] and Catalán *et al.* (SP, SdP, SA and SB)[12] multiparameter correlations have been used to describe solute–solvent interactions at both the ground and excited states. Those correlations take the form:

Kamlet-Abboud-Taft

$$\bar{\nu}_{max} = \bar{\nu}_0 + a \cdot \alpha + b \cdot \beta + p \cdot \pi^*$$

Catalán *et al.*

$$\bar{\nu}_{max} = \bar{\nu}_0 + csp \cdot SP + cdsp \cdot SdP + csa \cdot SA + csb \cdot SB$$

where $\bar{\nu}_{max}$ applies to absorption or emission.

In the Kamlet-Abboud-Taft equation α and β indicate the solvent hydrogen bond donating and accepting properties respectively, and π* is a measure of the nonspecific solvent polarity/polarizability, whereas a, b, and p are coefficients related to solute properties: a measures the tendency of the solute to donate a hydrogen bond to the solvent, b evaluates its ability to accept a hydrogen bond from the solvent, and p refers to the solute dipole moment.

Similarly, Catalán *et al.* proposed a generalized treatment of the solvent effect based on a set of four empirical, independent solvent scales, SdP, SP, SA, and SB characterize the dipolarity, polarizability, acidity, and basicity, respectively, of a certain solvent.

Kamlet–Abboud–Taft solvatochromic parameters α, β, and π* parameters come from ref. [57], and the Catalán's SA and SB parameters were collected from refs.[58-60], the Catalán solvent polarizability parameters SP were taken from ref. [61], and the recently proposed SdP solvent parameters come from ref. [62], and are compiled in Table SI3 of SI.

The statistical results of the Kamlet-Abboud-Taft and Catalán *et al.* multiparameter correlations are presented in Table 3. Kamlet-Abboud-Taft and Catalán *et al.* equations exhibit poor correlations for absorption. Although no quantitative conclusions can be drawn from the Kamlet-Abboud-Taft multiparameter correlation, the negative value of p_A regression coefficient indicates that the increase of the solvent polarity/polarisability (π*) yields a small red-shift in $\bar{\nu}_{max,A}$. On the other hand, coefficients a_A (< 0) and b_A (> 0) imply a blue shift in $\bar{\nu}_{max,A}$ for solvents with hydrogen bond donating capacity, and a red-shift in $\bar{\nu}_{max,A}$ as the hydrogen bond acceptor ability of the solvent increases, *i.e.* when the formation of a hydrogen bond with solvent lone pair(s) is facilitated. The fact a_A and b_A are higher than p_A indicate that solvent's acid-base properties are more important than its polarity/polarisability in affecting $\bar{\nu}_{max,A}$. Similar conclusions can be drawn from the Catalán *et al.* multiparameter correlation for absorption, the main difference being that solvent polarizability becomes the relevant effect (Table 3).

Better correlations are obtained for emission. In the case of Kamlet-Abboud-Taft equation the main effect, bathochromic, is attributed to the ability of asulam in accepting hydrogen bonds from the solvent. The hydrogen bond between protic solvents and the lone pair of the amino group in the S_0 state is broken on excitation, and the hydrogen bond is formed between the amino

proton and the lone pair of the solvent molecules. This is reflected by the positive values of the Kamlet's coefficients a in absorption spectra and the negative ones in fluorescence spectra. Here the increase in solvent polarity/polarisability causes a blue shift in $\bar{\nu}_{max,E}$.

As for Catalán *et al.* equation, the relevant factor is the stabilization of the excited state as the hydrogen bond donating ability of the solvent increases (Table 3), and the red shift in $\bar{\nu}_{max,E}$ due to the capability of asulam's hydrogens in forming hydrogen bonds with the solvent is approximately four-fold reduced. Contrary to absorption, an increase in the polarisability of the solvent destabilizes the excited state, whereas such change in its dipolarity has a small stabilizing effect. From the results of the effect of solvents dipolarity and polarizability on absorption and emission (Table 3), it follows that the ground state is more sensitive to those properties than the excited state.

Although Kamlet-Abboud-Taft and Catalán *et al.* fits are far from perfect, they are good enough to draw some interesting conclusions, and a bit more reliable than those involving bulk solvent polarity functions and of the microscopic solvent polarity parameter E_T^N

B. Theoretical description

Geometric changes

Upon excitation some geometrical changes take place on the amino group. A decrease in the planarity of the amino group is obtained in going from the ground state to the equilibrated excited states (Table 5), which implies less delocalization of the lone pair of the nitrogen atom onto the aromatic π system.

As shown in Fig. 6, the planarity of the amino group is defined in percent as $\{(A_1 + A_2 + A_3)/360^o\}\cdot 100$, A_i being the angles (º) C7-N10-H22 (A_1), C7-N10-H21 (A_2) and H22-N10-H21 (A_3). The decrease in the Mulliken's negative charge (Table SI4 of SI) on the amino nitrogen in

going from the ground state (- 0.7760) to excited states (FC = - 0.7144; S1 = - 0.7383) is in agreement with the increased amino group pyramidilization upon excitation.

Table 5. Relevant theoretical geometrical parameters of the amino group of the molecular form of asulam (**1**) (see the text and Fig. 6)

	S_0 / S_2 (^1L_a)	S_1 (^1L_b)	T_1 (^3L_a)	T_2 (^3L_b)
A_1 / º	116.59	112.79	112.38	113.52
A_2 / º	116.60	112.86	112.46	113.53
A_3 / º	113.02	109.65	109.05	110.46
(A_1+A_2+A_3) / º	346.21	335.3	333.89	337.51
% planarity	96.2	93.1	92.7	93.8
w_1 / º	-22.08	-29.58	-45.55	-27.7
w_2 / º	22.45	30.44	42.7	29.03
τ / º	0.2	0.4	-1.4	0.7
w_3 / º	177.6	176.0	155.7	176.3
$d_{C7\text{-}N10}$ / Å	1.385	1.397	1.402	1.390

The twist angle of the amino group is close to zero for all states, and the bond length between the phenyl ring and the amino group (C7-N10) follows the expected trend with excitation (Table 5). The twist angle of the amino group ($0º < \tau = (w_1 + w_2)/2 < 90º$) is calculated according to Ferreti et al.,[63] where the dihedrals angles (º) w_1 and w_2 are C2-C7-N10-H22 and C6-C7-N10-H21 respectively (Fig. 6).

On the other hand, the amino group is almost coplanar to the phenyl ring, but the lowest triplet state, where the nitrogen lies well above the plane defined by the carbons of the phenyl group

(Table 5), which is also consistent with its increased pyramidalization; the dihedral angle (º) w_3 (C5-C6-C7-N10) is used as a simple index of the planarity of the system formed by the phenyl ring and the nitrogen of the amino group (Fig. 6).

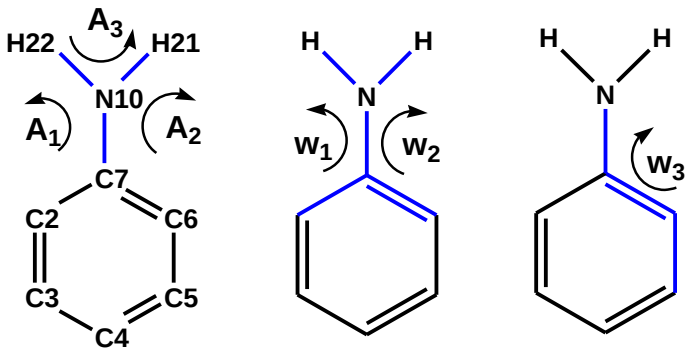

Figure 6. Blue lines indicate the atoms defining the angles involved in the determination of the planarity/pyramidalization of the amino group, its twist angle (τ), and the coplanarity (w_3) of the amino group and the phenyl ring around carbon-nitrogen (C7-N10) bond.

The increased pyramidalization of the amino group and the raise of the pKa (**1** ↔ **2** + H^+) upon excitation (pKa* > pKa) is consistent with the values found in the analysis of solvatochromic data according to Catalán *et al*. The change, from positive in absorption to negative in emission, of csa (Table 3), related to the ability of the solute to donate a hydrogen bond, is in agreement with both a less planar amino group and a more basic carbamate nitrogen. The contrary is expected, and observed, for csb, which measures the solute's tendency of accepting a hydrogen bond from the solvent, where its negative value is four-fold reduced in going from absorption to emission (Table 3).

Photophysics

The photophysics of asulam starts with absorption of near-UV radiation at the Franck-Condon (FC) ground-state geometry of the molecule. Two low-lying singlet excited states, labeled as S_1 (^1L_b ππ*) and S_2 (^1L_a ππ*) using Platt's nomenclature,[64] have been computed at the CASPT2 level at 4.36 (284 nm) and 5.02 eV (247 nm), respectively. The labeling derives from the composition of the CASSCF wave function as displayed in Table 6.

Table 6. Theoretical and experimental absorption spectrum of asulam

	Theoretical				Exp.
State	E_{VA}/eV(nm)[a]	*f*	μ/D	*Main configurations*	A_{max}/eV(nm)
S_0	–	–	5.51	–	–
T_1 (^3L_a ππ*)	3.64 (340)	–	5.20	H→L(53%); H-1→L+1(22%)	–
T_2 (^3L_b ππ*)	4.19 (296)	–	5.45	H→L+1(47%); H-1→L(31%)	–
T_3 (^3B_a ππ*)	4.27 (290)	–	5.74	H-1→L+1(57%); H→L(22%)	–
S_1 (^1L_b ππ*)	4.36 (284)	$<10^{-3}$	5.26	H→L+1(34%); H-1→L(27%)	–
T_4 (^3B_b ππ*)	5.01 (247)	–	7.71	H→L+1(29%); H-1→L(39%)	–
S_2 (^1L_a ππ*)	5.02 (247)	0.15	8.70	H→L (56%); H→L+1(15%)	4.64(265)[b]
S_3 (^1B_b ππ*)	6.51 (190)	0.17	5.89	H→L+1(21%); H-1→L(20%)	–

[a] CASPT2 vertical excitation energy at the FC geometry.

[b] Absorption band maximum in chloroform. Estimated oscillator strength: 0.43.

The transition to the S_1 (^1L_b $\pi\pi^*$) state, mainly described as the antisymmetric combination of the HOMO (H) $\rightarrow$ LUMO (L) + 1 (34%) and H - 1 $\rightarrow$ L (27%) one-electron promotions, has a corresponding oscillator strength lower than 10^{-3}. On the contrary, the S_2 (^1L_a $\pi\pi^*$) state, with a CASSCF wave function basically composed by the H $\rightarrow$ L (56%) configuration, has a related oscillator strength of 0.15 and, consequently, it will be the brigth state initially populated in this range of energies and from which the photochemical events will take place; this is also suported by the lack of mirror symmetry between the absorption and emission spectra (Fig. 3).

The absorption band maximum observed in chloroform at 4.68 eV (265 nm) is therefore clearly assigned to the S_2 (^1L_a $\pi\pi^*$) state. The vertical excitation energy, 5.02 eV (247 nm), computed in vacuo is, as usual, placed slightly higher than the band maximum. A third singlet excited state S_3 (^1B_b $\pi\pi^*$), formed by the symmetric combination of the H $\rightarrow$ L + 1 and H - 1 $\rightarrow$ L configurations, is computed much higher in energy, 6.51 eV (190 nm) with also a large related oscillator strength of 0.17. Regarding the triplet states, and as it is typical is π-conjugated organic molecules, a low-lying vertical excitation is computed for the T_1 (^3L_a $\pi\pi^*$) at 3.64 eV, well below the other states. Two other triplet states follow in energy, T_2 (^3L_b $\pi\pi^*$) and T_3 (^3B_a $\pi\pi^*$), at 4.19 (296 nm) and 4.27 eV (290 nm), respectively. A fourth triplet states is computed higher than the two lowest singlet states, at 5.01 eV (247 nm). The energy gap between the initially populated S_2 state (in the low-energy region of the spectrum) and the triplet states is large (>0.65 eV) except for T_4. As expected from the qualitative El Sayed rules,[65] all SOC terms are, however, too low in the FC region (<0.30 cm^{-1}) to promote efficient ISC processes, which should take place instead along the deactivation path of S_2. Certainly, all the states found at low-energies have a $\pi\pi^*$ character, and therefore SOC interaction is small, whereas $n\pi^*$ or $\pi\sigma^*$ states have been estimated much higher in energy.

The computed dipole moments of the different excited states are similar to that of the ground state, 5.51 D. Exceptions are the S_2 (^1L_a ππ*) and T_4 (^3B_b ππ*) states, which exhibit large dipole moments of 8.70 and 7.71 D, respectively. The analysis of the correlation between the Stokes shift (computed as difference between absorption and fluorescence maxima) in terms of bulk solvent polarity functions and of the microscopic solvent polarity parameter E_T^N (*vide supra*) yielded a difference of around 3 D (Table 3), supposedly between the ground and lowest singlet excited state dipole moments. In fact, as it will be shown later, the origin of the absorption and fluorescence bands relies on two different states, ^1L_a ππ* and ^1L_b ππ*, respectively. Despite such a large diferences and the estabilization undergone by the S_2 (^1L_a ππ*) band in presence of polar solvents, no relevant changes can be expected in the initial population pattern, considering the large gap between S_2 and the other states. As a matter of fact, and except for protic solvents like water, the absorption band maxima changes less than 0.1 eV in environments of different polarity.

In order to study the photophysical events, the main reaction decay pathway of the spectroscopic S_2 (^1L_a ππ*) state has to be determined. Figure 7 displays the CASPT2 energies of the low-lying singlet and triplet states of asulam obtained along the CASSCF MEP on the S_2 (^1L_a ππ*) state computed from the FC region. Although a small energy barrier can be observed along the path of the state, this feature has a minor significance because it is probably caused by unbalances between the initial S_0 DFT geometry, the computed CASSCF steepest-descendent MEP, and the CASPT2 point energies.

In essence the path can be considered essentially barrierless from the FC structure toward the region of the CI between the ground and the lowest singlet excited state, named $(gs/\pi\pi^*)_{CI}$ or $(S_0/S_1)_{CI}$ (S_1 now being the vertical S_2 state).

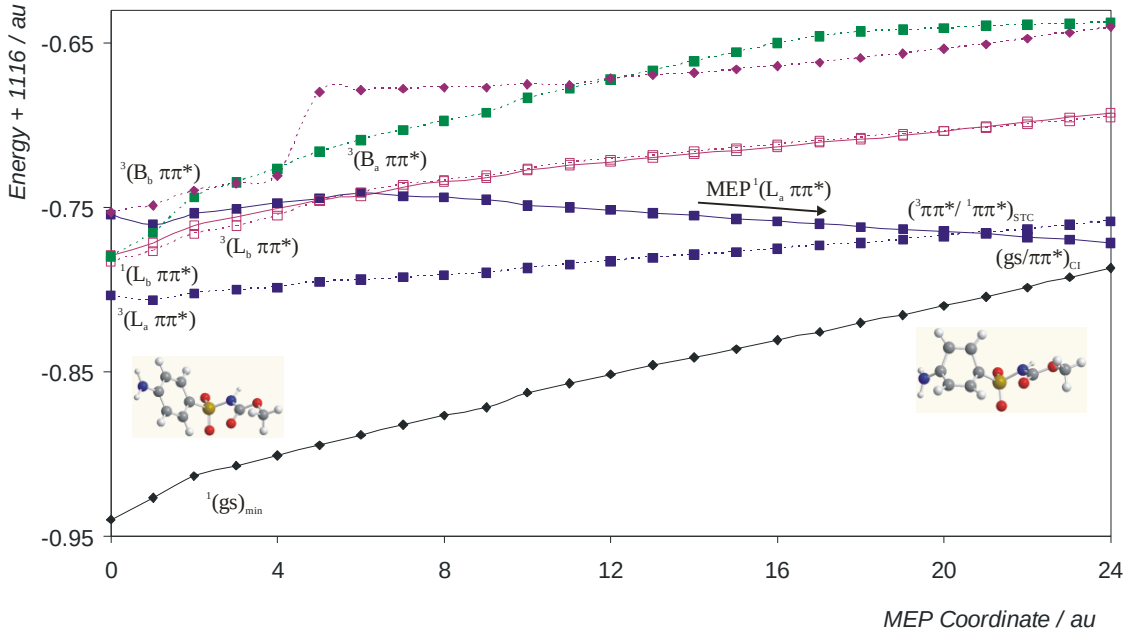

Figure 7. CASPT2 low-lying singlet and triplet states of asulam along the Minimum Energy Path computed from the FC geometry on the $^1(L_a\ \pi\pi^*)$ state of asulam. Singlet states (solid lines) and triplet states (dotted lines).

Figure 8 displays the geometries for asulam at the ground state minimum and at the $(gs/\pi\pi^*)_{CI}$ (see also Table SI5 of SI). The latter has been computed independently as a MECP between the S_0 and S_1 states and located at 4.12 eV (adiabatically from the ground state minimum) with a structure close to that of the molecule at the end of the MEP. The main distortion undergone by the system along the path has taken place on the benzene ring, which has adopted a boat-like $^{1,4}B$ conformation, [66] a diradicaloid-type structure known in the photochemistry of benzene to be a funnel for the radiationless decay to the ground state.[67]

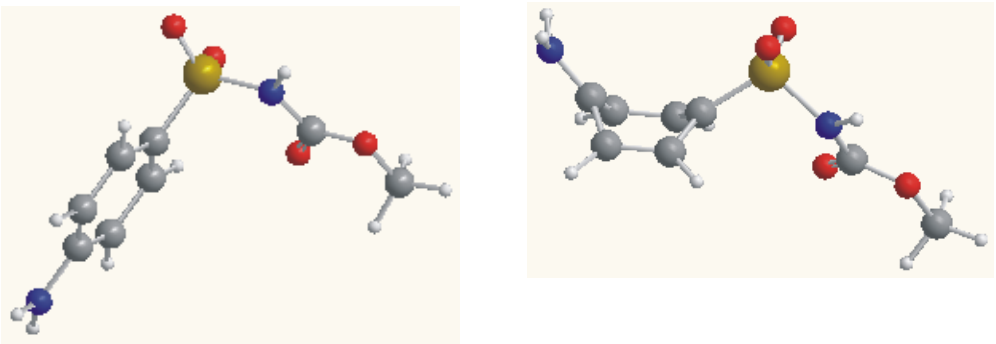

Figure 8. Optimized structures of asulam at the ground state minimum, (gs)min (left) and at the conical intersection $(gs/\pi\pi^*)_{CI}$ (right).

The singlet state relaxation along a barrierless path leading to conical intersections with two low-lying singlet states can be expected to be very efficient, and, correspondingly, the nonadiabatic decay effects in the CI regions. Several singlet and triplet states are crossed, however, during the evolution of the system, and efficient population transfer can take place (see Fig. 7) near the crossing regions. Close to point 5 of the MEP a degeneracy region between the S_2 (^1L_a $\pi\pi^*$) and S_1 (^1L_b $\pi\pi^*$) states occurs. From this point, a MEP computed on the S_1 (^1L_b $\pi\pi^*$) state hypersurface (see SI, Fig.S18) leads directly to the minimum of the state, computed adiabatically at 4.39 eV (T_e, 282 nm) with a vertical emission of 4.07 eV (304 nm). Such values can be successfully compared with the fluorescence data obtained in chloroform, yielding band origins and maximum of 4.13 eV (T_0, 300 nm) and 3.83 eV (323 nm), respectively (see Table 7). As the agreement is good enough and no low-lying energy minimum has been located for the S_2 (^1L_a $\pi\pi^*$) state, it can be safely assumed that the S_1 (^1L_b $\pi\pi^*$) state is the protagonist of the fluorescence. The state minimum displays a dipole moment similar to that of the ground state (4.91 D), and therefore the emission band should not be strongly affected by the polarity of the solvent. Indeed, the fluorescence maximum shifts by less than 0.1 eV in different environments.

Table 7. Theoretical and experimental absorption and emission spectrum of asulam.

State	Theoretical /eV (nm)			Experimental /eV (nm)		
	E_{VA}[a]	T_e[a]	E_{VE}[a]	A_{max}[b]	T_0[b]	E_{max}[b]
T_1 (^3L_a ππ*)	3.64 (340)	3.61 (343)	2.78 (445)	–	3.44 (360)[c,d]	2.82 (439)[c,d]
T_2 (^3L_b ππ*)	4.19 (296)	4.23 (292)	3.92 (316)	–	–	–
T_3 (^3B_a ππ*)	4.27 (290)	–	–	–	–	–
S_1 (^1L_b ππ*)	4.36 (284)	4.39 (282)	4.07 (304)	–	4.13 (300)[c,f]	3.83 (323)[c,f]
S_2 (^1L_a ππ*)	5.01 (247)	–[g]	–[g]	4.68 (264)[c]	–	–
T_4 (^3B_b ππ*)	5.02 (247)	–	–	–	–	–
S_3 (^1B_b ππ*)	6.51 (190)					

[a] CASPT2 vertical excitation energy (E_{VA}), electronic band origin (T_e), and vertical emission energy (E_{VE}).

[b] Measured absorption band maximum (A_{max}), band origin (T_0), and fluorescence maximum (E_{max}).

[c] In water (T_1) and chloroform (S_1 and S_2).

[d] Computed (3858 ns) and experimental (6.25 ns) fluorescence radiative lifetime ($\tau_{F\ rad}$). The Strickler-Berg model is then not applicable here due to the high nonradiative rates. See text.

[e] Oscillator strengths $<10^{-3}$, 0.15, and 0.17, respectively.

[f] Computed (83.4 s) and experimental (2.58 s) phosphorescence radiative lifetime ($\tau_{P\ rad}$).

[g] For the isolated molecule the MEP on S_2 (^1L_a ππ*), after crossing with all other excited states, leads directly to a conical intersection with the ground state, $(S_0/S_1)_{CI}$ placed adiabatically at 4.12 eV.

Fluorescence in asulam is, however, weak. The emission quantum yield ϕ_F has been measured to increase with the polarity of the solvent: 0.032 in acetonitrile, 0.099 in ether, and 0.155 in

water. Considering the low sensitivity of the S_1 (^1L_b ππ*) emission band on the solvent polarity, the increase on the quantum yield should be related to the stabilization of the highly polar S_2 (^1L_a ππ*) state and, accordingly, of the conical intersection $(S_1/S_2)_{CI}$ triggering the population switch from S_2 to S_1 along the decay of the higher singlet state. The low fluorescence quantum yield also points to the presence of efficient nonradiative decay channels. It is not surprising then that the theoretical fluorescence radiative lifetime, computed by means of the Strickler-Berg approximation as 3858 ns (as a logical consequence of the low transition dipole moment relating S_0 and S_1) cannot be compared with the estimated value in water, 6.25 ns. It is well known that the Strickler-Berg approximation is not applicable to systems with predominant nonradiative pathways.[26,42,43]

Along the evolution through the S_2 (^1L_a ππ*) state decay four triplet states are crossed, one at the beginning (~5.0 eV), T_4 (^3B_b ππ*), then T_3 (^3B_a ππ*) and T_2 (^3L_b ππ*), and finally the T_1 (^3L_a ππ*) state close to the end of the path (~4.5 eV), that is, near the conical intersection $(gs/\pi\pi^*)_{CI}$ and displaying therefore a similar structure. The computed electronic SOC terms between the S_2 (^1L_a ππ*) and the different triplet states at the corresponding STC regions are somewhat low (<0.3 cm^{-1}), although such values are probably underestimated because the relative small number of states included in the coupling (four singlet and four triplet states, all of ππ* type). In any case the computed overall ISC rate at each of the STC regions is expected to become large enough to guarantee efficient processes once the vibrational effects and density of states are taken into account in the SOC coupling, as it has been established in a number of systems.[68] We have followed respective MEPs from the STC crossings between S_2 (^1L_a ππ*) and T_2 and T_1, which display the largest SOC values in the respective crossing regions (~0.3 cm^{-1} in both cases). The T_2 state evolves toward its minimum, as shown by computing the corresponding MEPs (see SI,

Fig. SI9), and finally it decays to the lowest T_1 triplet state through an efficient triplet-triplet IC processes, because the corresponding $(T_2/T_1)_{CI}$ lies close by the T_2 minimum (see SI Fig. SI10). The second MEP computed leads the T_1 (^3L_a $\pi\pi^*$) from the $(S_2/T_1)_{STC}$ towards the triplet state minimum (see SI, Fig. SI11). In either case – IC from T_2 or ISC from S_2 – the T_1 (^3L_a $\pi\pi^*$) will decay to its own minimum and become phosphorescent (see Fig. 9).

These ISC mechanisms, surely enhanced in polar solvents, may explain the large triplet formation quantum yield determined in water as 0.84. Considering the different energy ranges in which the STC regions are located it can be expected for the triplet quantum yield to be wavelength dependent, an effect and a mechanism present in molecules like thymine, uracil or adenine.[69,70] Regarding the parameters computed for the phosphorescence, the band origin, 3.61 eV (T_e, 343 nm), and vertical emission, 2.78 eV (445 nm), are in good correspondence with the experimental values in water, 3.44 (360) and 2.82 eV (439 nm), respectively.

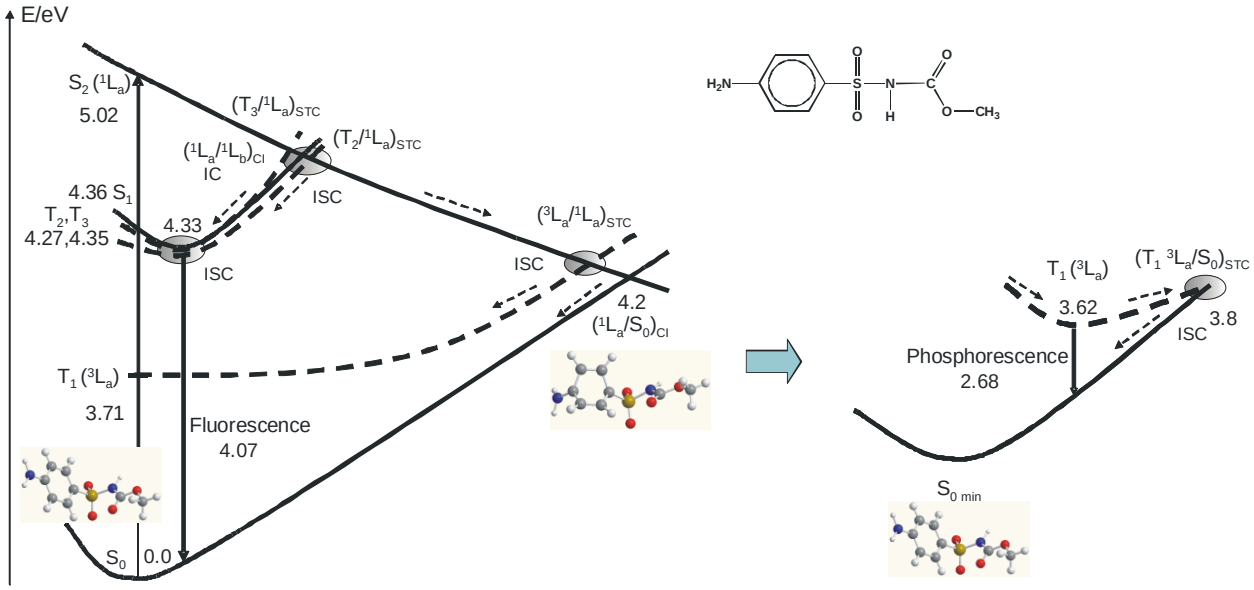

Figure 9. Scheme of photophysics of asulam based on the CASPT2 results

The theoretically derived phosphorescence radiative lifetime, 83.4 s, is one order of magnitude larger than the experimental estimation in water, 2.58 s. As for the fluorescence, although in minor extent, the discrepancy can be attributed to the presence of important nonradiative relaxation processes. Indeed, as the phosphorescence quantum yield (ϕ_P) is determined in water to be ϕ_P 0.36, and comparing with the total triplet formation, 84%, a high yield of deactivation to the ground state ϕ_{TS} 0.48 is established. Accordingly to that, from the T_1 minimum the system may reach an intersystem crossing region between the T_1 and the ground state, (^{1}gs/^3L_a $\pi\pi^*$)$_{STC}$, surmounting a small barrier of 0.41 eV (~10 kcal mol^{-1}) (see SI, Fig. SI12). The ISC funnel, in which the electronic SOC has been computed as 0.86 cm^{-1} favoring then the energy transfer, is easily accessible with the available excess energy, and the large ratio of radiatonless decay can be therefore understood.

The presented photoprocesses that the system may undergo are resumed in Figure 9, which displays a scheme of the photophysics of asulam based on CASPT2 results. Once more the CASPT2 method reveals more appropriate to describe excited states than lower-level methods used in the past with this compound.[71,72]

Finally notice that the main charge transfer takes place between C4 and C7 (Table SI4 of SI); in going from the ground to the S_2 (^1L_a $\pi\pi^*$) state at the FC geometry C4 doubles its negative charge, and then suffers a three-fold reduction at S_1 (^1L_b $\pi\pi^*$); on the other hand C7 becomes twice its positive charge at S_2 (^1L_a $\pi\pi^*$) state at the FC geometry, which reduces 6-fold at S_1 (^1L_b $\pi\pi^*$); the charge separation, larger at the S_2 state at the FC region than at the minimum of S_1 state, is consistent with the higher dipole moment calculated for S_2.

Conclusions

Experimental and quantum chemistry methods, at the CASPT2 level, were used for studying of the photophysical behavior of asulam, mainly in its molecular form (2). Absorption maximum wavelengths, ascribed to a $\pi \rightarrow \pi^*$ aromatic electronic transition, showed a weak red-shift upon increasing the polarity of the solvent, but for water and ethanol, whereas its fluorescence emission peak underwent a larger red-shift as solvent polarity rises.

Linear regressions analyzing solvent effects on absorption and fluorescence spectra with the solvatochromic method in terms of bulk polarizability of the solvent, or including solute-solvent specific interactions (multiparamenter approaches of Kamlet-Abboud-Taft and Catalán et al.), do not give specially good results, likely due to the existence of many sites able to specifically interact with the solvent. Results from those multiparameter approaches are consistent with the observed increase in pKa in going from the ground state to the excited state, ΔpKa (= pKa* – pKa) c.a. 3.

Red-shifts on increasing the solvent polarity implies that the ground state is less polar than the excited singlet-state ($\mu_g < \mu_e$), which is consistent with the increase of the dipole moment determined by both empirically from solvatochromic data and theoretically at the CASPT2 level. This confirms again that the excited singlet-state of asulam is more polar than the ground state, and, therefore, more sensitive to solvent effects. Comparison of the modified absorption and the fluorescence spectra shows a lack of mirror image symmetry, which reflects different nuclear configurations in the absorbing and emitting states. The same conclusion is derived from either the experimental transition dipole moments or the theoretical calculations, two distinct electronic transitions have to be considered for absorption and emission. Two low-lying singlet excited states, labeled as S_1 (^1L_b $\pi\pi^*$) and S_2 (^1L_a $\pi\pi^*$) have been characterized; the absorption band maximum has been assigned to the S_2 (^1L_a $\pi\pi^*$) state, whereas the lowest-lying state S_1 (^1L_b $\pi\pi^*$)

is responsible for the fluorescence spectrum. Fluorescence quantum yield at room temperature is low and varies with the solvent, highest in water ($\phi_f = 0.16$) and independent of the medium's acidity ($3 < pH < 11$), and lowest in methanol and 1-propanol ($\phi_f\ c.a.\ 0.02$). Fluorescence lifetime in aqueous solution is 1 ns ($k_f = 1.5 \cdot 10^{-8}\ s^{-1}$). There is an efficient intersystem crossing as follows from the phosphorescence quantum yield found in glassy ETOH ($\phi_P = 0.36$) at 77 K, the phosphorescence lifetime being 1.1 s ($k_P = 0.4\ s^{-1}$); thus, the remaining 48% decays through non-radiative pathways. Charge reorganization upon excitation mainly involves changes between two carbon atoms of the aromatic ring, with a small participation of the nitrogen of the amino group.

The decay pathway of the spectroscopic S_2 (^1L_a $\pi\pi^*$) state can be considered essentially barrierless from the FC structure toward the region of the internal conversion between the ground and the lowest singlet excited state, $(gs/\pi\pi^*)_{CI}$. The main geometrical distortion undergone by the system is the diradicaloid-type structure of the benzene ring, which is known to be a funnel for the radiationless decay to the ground state. Along the main decay path, the presence of a conical intersection between the two low-lying singlet excited state states switched part of the population to the fluorescent (^1L_b $\pi\pi^*$) state, which decays to its emitting minimum. Different intersystem crossing regions have been also characterized on the potential energy hypersurface connecting the FC region and the $(gs/\pi\pi^*)_{CI}$, which account for the large triplet formation quantum yield determined in water ($\Phi_T = 0.84$), as well as the phosphorescent features experimentally detected.

Molecular-level understanding of the underlying photophysics provides an advantage in the design of new biocides with improved properties.

Acknowledgments

Financial support is acknowledged from projects CTQ2007-61260, CSD2007-0010 Consolider-Ingenio in Molecular Nanoscience of the Spanish MEC/FEDER, and PGIDIT05TAM10301PR of the Xunta de Galicia (Spain). Thanks are given to the Centro de Supercomputación de Galicia (CESGA) for computing facilities. AFC acknowledges the research grant (Formación Personal Investigador) of the former Spanish Ministerio de Educación y Ciencia. Finally, we wish to thank Prof. Dr. Manuela Merchán (University of Valencia) for proof reading the manuscript.

Supporting Information. Additional computational details, Figures SI1 to SI12, and Tables SI1 to SI5. This material is available free of charge via the Internet at http://pubs.acs.org.

References

(1) Jha, M. N.; Mishra, S. K. Bulletin of Environmental Contamination and Toxicology **2005**, 75, 316-323.

(2) Gevao, B.; Semple, K. T.; Jones, K. C. Environmental Pollution **2000**, 108, 3 -14.

(3) EFSA Journal **2010**, 8, 1822.

(4) Tomašević, A. V.; Gašić, S. M. In Insecticides – Basic and Other Applications; Larramendy, S. S. M., Ed.; InTech: Rijeka (Croatia), 2012, pp 39 - 60.

(5) Catastini, C.; Sarakha, M.; Mailhot, G.; Bolte, M. Science of the Total Environment **2002**, 298, 219-228.

(6) *www.epa.gov/oppsrrd1/REDs/0265.pdf* **1995**, EPA 738-R-95-024.

(7) Kawski, A.; Bojarski, P. Spectrochimica Acta Part A **2011** 82, 527- 528.

(8) Kamlet, M. J.; Abboud, J. L.; Abraham, M. H.; Taft, R. W. J. Org. Chem. **1983**, 48, 2877.

(9) Kamlet, M. J.; Abboud, J. L.; Taft, R. W. J. Am. Chem. Soc. **1977**, 99, 6027 - 6038.

(10) Kamlet, M. J.; Dickinson, C.; Taft, R. W. Chem. Phys. Lett. **1981**, 77, 69 - 72.

(11) Marcus, Y.; Kamlet, M. J.; Taft, R. W. J. Phys. Chem. **1988**, 92, 3613 - 3622.

(12) Catalán, J.; de Paz, J. L. G.; Reichardt, C. J. Phys. Chem. A **2010**, 114, 6226 - 6234.

(13) Merchán, M.; Serrano-Andrés, L. In Computational Photochemistry; 1st. ed.; Olivucci, M., Ed.; Elsevier: Amsterdam, The Netherlands, 2005; Vol. 16, pp 35 - 91.

(14) Serrano-Andrés, L.; Merchán, M. In Radiation Induced Molecular Phenomena in Nucleic Acids; Leszczynski, J., Shukla, M., Ed.; Springer: The Netherlands, 2008, pp 435 - 472.

(15) Giussani, A.; Merchán, M.; Roca-Sanjuán, D.; Lindh, R. J. Chem. Theory Comput. **2011**, 7, 4088 - 4096.

(16) Williams, A. T. R.; Winfield, S. A.; Millar, J. N. Analyst **1983**, 108, 1067 - 1071.

(17) Murov, S. L.; Carmichael, I.; Hug, G. L. Handbook of Photochemistry; Marcel Dekker, Inc.: New York, 1993.

(18) Roos, B. O.; Fülscher, M. P.; Malmqvist, P.-Å.; Serrano-Andrés, L.; Pierloot, K.; Merchán, M. Adv. Chem. Phys. **1996**, 93, 219 - 331.

(19) Serrano-Andrés, L.; Merchán, M.; Nebot-Gil, I.; Lindh, R.; Roos, B. O. J. Chem. Phys. **1993**, 98, 3151 - 3162.

(20) Serrano-Andrés, L.; Merchán, M.; Borin, A. C. Proc. Natl. Acad. Sci. USA. **2006**, 103, 8691 - 8696.

(21) Serrano-Andrés, L.; Merchán, M.; Lindh, R. J. Chem. Phys. **2005**, 122, 104 - 107.

(22) Aquilante, F.; De Vico, L.; Ferré, N.; Ghigo, G.; Malmqvist, P.-Å.; Pedersen, T.; Pitonak, M.; Reiher, M.; Roos, B. O.; Serrano-Andrés, L.; Urban, M.; Veryazov, V.; Lindh, R. J. Comp. Chem. **2010**, 31, 224 - 247.

(23) Gaussian 09, R. A., Frisch, M. J.; Trucks, G. W.; Schlegel, H. B.; Scuseria, G. E.; Robb, M. A.; Cheeseman, J. R.; Scalmani, G.; Barone, V.; Mennucci, B.; Petersson, G. A.; Nakatsuji, H.; Caricato, M.; Li, X.; Hratchian, H. P.; Izmaylov, A. F.; Bloino, J.; Zheng, G.; Sonnenberg, J. L.; Hada, M.; Ehara, M.; Toyota, K.; Fukuda, R.; Hasegawa, J.; Ishida, M.; Nakajima, T.; Honda, Y.; Kitao, O.; Nakai, H.; Vreven, T.; Montgomery, Jr., J. A.; Peralta, J. E.; Ogliaro, F.; Bearpark, M.; Heyd, J. J.; Brothers, E.; Kudin, K. N.; Staroverov, V. N.; Kobayashi, R.; Normand, J.; Raghavachari, K.; Rendell, A.; Burant, J. C.; Iyengar, S. S.; Tomasi, J.; Cossi, M.; Rega, N.; Millam, N. J.; Klene, M.; Knox, J. E.; Cross, J. B.; Bakken, V.; Adamo, C.; Jaramillo, J.; Gomperts, R.; Stratmann, R. E.; Yazyev, O.; Austin, A. J.; Cammi, R.; Pomelli, C.; Ochterski, J. W.; Martin, R. L.; Morokuma, K.; Zakrzewski, V. G.; Voth, G. A.; Salvador, P.; Dannenberg, J. J.; Dapprich, S.; Daniels, A. D.; Farkas, Ö.; Foresman, J. B.; Ortiz, J. V.; Cioslowski, J.; Fox, D. J. Gaussian, Inc., Wallingford CT, 2009.

(24) Vulliet, E.; Emmelin, C.; Chovelon, J.-M. J. Photochem. & Photobiol. A: Chemistry **2004**, 163, 69 - 75.

(25) Bridges, J. W.; Williams, R. T. Biochem. J. **1968**, 107, 225 - 237.

(26) McHale, J. L. Molecular Spectroscopy; Prentice Hall: New Jersey,, 1999.

(27) Srividya, N.; Sinha, A.; TAP, R. J. Solution Chem. **2000**, 29, 847 - 857.

(28) Williams, R. T.; Bridges, J. W. J. Clin. Path. **1964**, 17, 371 - 394.

(29) Birks, J. B. Photophysics of Aromatic Molecules; Wiley, New York., 1970.

(30) Gutavsson, L.; Cassara, V.; Gulbinas, G.; Gurzadyan, J.-C.; Mialocq, S.; Pommeret, M.; Sorguis, P. v. d. M. J. Phys. Chem. A **1998**, 102, 4229 - 4245.

(31) Saha, S. K.; Dogra, S. K. J. Photochem. Photobiol. A: Chem. **1997**, 110, 257 - 266.

(32) Köhler, G. J. Photochem. **1987**, 38, 217 - 238.

(33) Bridges, J. w.; Gifford, L. A.; Hayes, W. P.; Miller, J. N.; Burns, D. T. Anal. Chem. **1974**, 46, 1010 - 1017.

(34) Förster, T. Z. Electrochem. **1950**, 54, 531 - 535.

(35) Jaffé, H. H.; Jones, H. L. J. Org. Chem. **1965**, 30, 964 - 969.

(36) Venning, D. R.; Mousa, J. J.; Luka siewicz, R. J.; Winefordner, J. D. Anal. Chem. **1972**, 44, 2387 - 2389.

(37) Tobita, S.; Ida, K.; Shiobara, S. Res. Chem. Intermed. **2001**, 27, 205 - 218.

(38) Saito, F.; Tobita, S.; Shizuka, H. J. Chem. Soc. Faraday Trans. **1996**, 92, 4177 - 4185.

(39) Forbes, W. F. Can. J. Chem. **1960**, 38, 896 - 910.

(40) Kochemirovskii, A. S. Opt. Spectrosc. **1960**, 8, 206.

(41) Blais, J.; Gauthier, M. J. Photochem. **1978**, 9, 529 - 538.

(42) Strickler, S. J.; Berg, R. A. J. Chem. Phys. **1962**, 37, 814.

(43) Rubio-Pons, O.; Serrano-Andrés, L.; Merchán, M. J. Phys. Chem. A. **2001**, 105, 9664 - 9673.

(44) Turro, N. J. Modern Molecular Photochemistry; University Sciences Books, 1991.

(45) Land, E. J.; Navaratnam, S.; Parson, B. J.; Philips, G. O. Photochem. Photobiol. **1982**, 35, 637 - 642.

(46) Bakhshiev, N. G. J. Opt. Technol. **2001**, 68, 184 - 188.

(47) Jozefowicz, M.; Milart, P.; Heldt, J. R. Spectrochim. Acta, Part A **2009**, 74, 959 - 963.

(48) Reichardt, C. Solvents and Solvent effects in Organic Chemistry; Wiley-VCH, 2003.

(49) Suppan, P.; Ghoneim, N. Solvatochromism; Royal Society of Chemistry, 1997.

(50) Lippert, E. Z. Naturforsch. **1955**, 109, 571 - 578.

(51) Lippert, E. Z. Elektrochem. **1957**, 61, 962 - 975.

(52) Mataga, N.; Kaifu, Y.; Koizumi, M. Bull. Chem. Soc. Jpn. **1955**, 28, 690 - 691.

(53) Mataga, N.; Kaifu, Y.; Koizumi, M. Bull. Chem. Soc. Jpn. **1956**, 29, 465 - 470.

(54) Köhler, G. J. Photochem. **1987**, 38, 217 - 238.

(55) Ledger, M. B.; Suppan, P. Spectrochim Acta. A **1967**, 23, 3007 - 3011.

(56) Rechthaler, K.; Köhler, G. Chem. Phys. Lett. **1994**, 189, 99 -116.

(57) Marcus, Y. Chem. Soc. Rev. **1993**, 22, 409 - 416.

(58) Catalán, J.; G.Wypych, Ed.; ChemTec Publishing: Toronto, 2001, pp 583 - 616.

(59) Catalán, J.; Díaz, C. Liebigs Ann./Recl. **1997**, 1941 - 1949.

(60) Catalán, J.; Díaz, C.; López, V.; Pérez, P.; de Paz, J. L. G.; Rodriguez, J. G. Liebigs Ann./Recl. **1996**, 1785 - 1794.

(61) Catalán, J.; Hopf, H. Eur. J. Org. Chem. **2004**, 4694 - 4702.

(62) Catalán, J. J. Phys. Chem. B **2009**, 113, 5951 - 5960.

(63) Ferretti, V.; Bertolasi, V.; Cilli, P.; Cilli, C. J. Phys. Chem. **1993**, 97, 13568 - 13574.

(64) Platt, J. R. J. Chem. Phys. **1949**, 17, 489.

(65) Lower, S. K.; El-Sayed, M. A. Chem. Rev. **1966**, 66, 199 - 241.

(66) Evans, D. G.; Boeyens, J. C. A. Acta Cryst. B **1989**, 45, 581 - 590.

(67) Palmer, I. J.; Ragazos, I. N.; Bemardi, F.; Olivucci, M.; Robb, M. A. J. Am. Chem. Soc. **1993**, 115, 673 - 682.

(68) Tatchen, J.; Gilka, N.; Marian, C. M. Phys. Chem. Chem. Phys. **2007**, 9, 5209 - 5221.

(69) Climent, T.; González-Luque, R.; Merchán, M.; Serrano-Andrés, L. Chem. Phys. Lett. **2007**, 441, 327 - 331.

(70) Serrano-Pérez, J. J.; González-Luque, R.; Merchán, M.; Serrano-Andrés, L. J. Phys. Chem. B **2007**, 111, 11880 - 11883.

(71) Bazyl, O. K.; Chaikovskaya, O. N.; Artyukhov, V. Y. Optics and Spectroscopy **2005**, 98, 838 - 843.

(72) Bazyl, O. K.; Chaikovskaya, O. N.; Artyukhov, V. Y.; Maier, G. V. Optics and Spectroscopy **2004** 97, 42-47.